2019-2020 Australian bushfire smoke, multi-year La Niña, and implications for the Interdecadal Pacific Oscillation (IPO)

Check for updates

Gerald A. Meehl[1] ✉, John Fasullo[1], Sasha Glanville[1], Antonietta Capotondi[2], Julie M. Arblaster[3], Aixue Hu[1], Nan Rosenbloom[1] & Stephen Yeager[1]

The onset of a La Niña event in 2020, with a major contribution from the huge amounts of smoke produced by the disastrous 2019–2020 Australian bushfires, resulted in that event persisting over the next several years with significant impacts worldwide. Here, we attempt to understand the processes and mechanisms related to the wildfire smoke that could have sustained this multi-year high-impact event by analyzing initialized Earth system predictions with E3SMv2 and CESM2 with and without the effects of the Australian bushfire smoke. We hypothesize that Bjerknes feedback sustains the La Niña conditions through an intensified anomalous Walker Circulation that connects strengthened precipitation and ascent in the western Pacific with anomalous subsidence, an invigorated South Pacific High, stronger Trades, and cooler SSTs across the tropical Pacific. Some ensemble members transition to El Niño after 2 years, driven by the development of a positive North Pacific Meridional Mode (NPMM) near Hawaii. Coupled processes in the off-equatorial western Pacific Ocean indicate a connection to the negative phase of the Interdecadal Pacific Oscillation with implications for understanding and predicting interannual and decadal Earth system fluctuations.

The triple-dip La Niña of the early 2020s had profound climate impacts across many regions across the globe, including excessive flooding in Australia[1] and severe drought over the western U.S.[2,3]. Consequently, there have been efforts to understand the mechanisms involved with the onset and duration of the event[3]. There could also be connections between interannual and decadal timescales in the tropical Pacific. ENSO events on the inter-annual timescale could contribute to transitions of the Interdecadal Pacific Oscillation (IPO), a dominant mode of decadal timescale variability with ENSO-like SST anomaly patterns in the tropical Pacific[4]. Such understanding is essential to improving predictability and consequent societal resilience to such high-impact events.

Indications of an onset of a La Niña event were predicted with 1–8 months lead times[5], but the intensity and duration of the multi-year La Niña event were poorly predicted[6], and consequently, the event was deemed somewhat unusual. Though multi-year La Niña events are not unprecedented[3,5,7], such events are somewhat rare and are sometimes[8], but not always[9], preceded by a strong El Niño that preconditions warm water volume through the discharge oscillator mechanism. But the 2020 onset of the triple-dip La Niña was not preceded by a strong El Niño event[10]. Additionally, the roughly 40-year tendency for tropical Pacific SSTs to become more La Niña-like[5,11] from positive IPO conditions in the 1980s and

early 1990s to negative IPO after about 2000[12] makes the Pacific more susceptible to multi-year La Niña events[13]. Forcing of the Pacific through the atmospheric Walker Circulation connection to the Indian and Atlantic Oceans has also been postulated as playing a role[10,14,15].

Evidence has been presented from models and observations that a chain of coupled processes connected to the Australian wildfire smoke likely contributed to the onset and intensity of the La Niña event in 2020[6,16]. This evidence has shown that the wildfire smoke was advected across the Pacific to brighten clouds off the west coast of South America and reduce incoming solar radiation at the surface to lower SSTs there. Those cooler SSTs dried the boundary layer, and the reduced moist static energy at low levels was advected by the southeast Trade Winds into the equatorial eastern Pacific, where SSTs cooled, the ITCZ shifted northward, and coupled feedbacks amplified the cooling, with the end product being a La Niña event[6,16]. While those model simulations predicted a La Niña-like state, the wildfire smoke intensified and lengthened the simulated event (ref. 6, their Fig. 2a).

Though the effects of the smoke had long dissipated as the La Niña event reached the end of its first year, the negative SST anomalies in the eastern equatorial Pacific strengthened and spread across the Pacific, reaching the western equatorial Pacific. While 2-year La Niña events are not uncommon[8], this La Niña event then continued into a third year[3,17].

[1]National Center for Atmospheric Research, Boulder, CO, USA. [2]CIRES and NOAA Physical Sciences Laboratory, University of Colorado, Boulder, CO, USA. [3]ARC Centre of Excellence for Climate Extremes, Monash University, Melbourne, VIC, Australia. ✉e-mail: meehl@ucar.edu

Thus, the question we address here is: what were the effects of Australian wildfire smoke on the subsequent multi-year time evolution of the tropical Pacific system? Our intention is not to simulate the multi-year La Niña per se, but to perform an initialized hindcast sensitivity experiment. This is an important distinction that we need to emphasize. Therefore, the timing of our year designations is tied to the timing of the sensitivity experiment with an initialization on August 1, 2019, just prior to the start of the wildfires. Our "lead year 1" from August 2019 to July 2020 is the first full year that the wildfire smoke could affect the hindcast sensitivity experiment outcome. Therefore, we intend to elucidate the processes that sustained the La Niña event with connections to the Australian wildfire smoke that can be studied in an Earth system predictability context.

Here we perform two sets of retrospective 3-year initialized Earth system predictions (hindcasts) with two Earth system models, CESM2 and E3SMv2, to explore structural uncertainties in the climate response[6] (see "Methods"). Both models have comparable resolution of about 100 km, but have different atmosphere and ocean model components that are likely related in part to the ENSO amplitude in CESM2 being about twice that in E3SMv2. Both sets are initialized in August 2019, and integrated for three model years to July 2022. Each has 30 ensemble members with the "smoke" ensembles using observed biomass emissions over Australia and climatological emissions elsewhere, and the "no-smoke" ensembles using climatological emissions globally. Results here are shown for annual averages, August to July, computed as differences "smoke minus no-smoke" to see what effects the wildfire smoke had on the prediction. CESM2 and E3SMv2 both include aerosol schemes whereby cloud condensation nuclei (CCN) and cloud albedo can be affected by smoke aerosols such that the presence of smoke aerosols generally makes clouds brighter[6,16]. The no-smoke simulations are from the standard Seasonal-to-Multi-year Large Ensemble (SMYLE) initialized hindcasts with CESM2 and E3SMv2 and use a climatology of biomass burning emissions[18]. The observed Australian bushfire smoke emissions from the Global Fire Emissions Database (GFED) are included in the "smoke" hindcasts and use monthly-mean observed biomass burning emissions.

The response of cloud albedo and net solar radiation at the surface to the wildfire smoke in the two models (Fig. S1) confirms previous results[6] in that the effect of the smoke is to increase cloud albedo in the eastern subtropical Pacific and reduce net solar radiation at the surface there as a consequence. The magnitude of the response in CESM2 in the key cloud area of equator to 30°S, 80°W to 110°W[6] shows an increase in cloud albedo in CESM2 (about +0.04), roughly twice that in E3SMv2 (about +0.02) (Fig. S1a, b). Meanwhile, those increases in cloud albedo from the cloud-aerosol response to the wildfire smoke advected across the subtropical Pacific from Australia result in a decrease of net solar radiation at the surface of -20 Wm^{-2} in CESM2 and roughly -10 Wm^{-2} in E3SMv2 (Fig. S1c, d). This decrease would contribute to a greater decrease of SSTs in CESM2 compared to E3SMv2, and contribute to the different magnitude of the SST response in the two models[6]. This stronger cloud feedback response in CESM2 is consistent with the finding that CESM2 has one of the strongest responses of low cloud-SST feedback of all the CMIP6 models[19].

Our hindcast "lead years" run from August 1 to July 31, while canonical "La Niña years" typically run from April to March[3]. Thus, the observed triple-dip La Niña event reached the La Niña SST anomaly threshold in the northern summer of 2020[3], so our model sensitivity experiment lead year 1 captures conditions leading up to the onset of the event, while our lead years 2 and 3 simulate processes that sustained the La Niña past the first year. Other studies describing multi-year La Niña events[3,7] use different year designations, ranging from calendar years[7] to canonical La Niña years from April to March[3]. Later, we will describe extensions to the initial model sensitivity experiments to address the end of the observed triple-dip La Niña event in early 2023 after our lead year 3 ended. Finally, since these are model sensitivity experiments, our anomalies are computed as "smoke minus no-smoke," which can differ from anomalies computed for observations using a time period of interest minus a climatology. Consequently, the magnitudes of anomalies from the model sensitivity experiments and observations are

qualitatively comparable, but the patterns of the anomalies are more indicative of the processes we are describing compared to the pattern of observed anomalies.

Results

Tropical Pacific cooling in the lead years 2 and 3 in the models

After the initial cooling response of SSTs in the equatorial eastern Pacific in lead year 1 in both models (Fig. 1a, b, August 2019–July 2020), negative SST anomalies spread across the Pacific in lead year 2 with significant anomalies of about -0.6 °C (Fig. 1c, d, August 2020–July 2021) as documented previously for CESM2[6] and seen here for E3SMv2 as well. The anomalies in the latter have the same pattern, but about half the amplitude of those in CESM2. There are indications of negative North and South Pacific Meridional Modes (NPMM; SPMM)[20–22] in lead year 2 in both models, with characteristically negative SST anomalies arcing from the deep tropics to the northeast and southeast into the subtropical eastern Pacific. This is consistent with previous results that have pointed to negative NPMM and SPMM that likely helped prolong the observed triple-dip La Niña event[7,23–25]. The results here suggest further that such anomalies may have been partially influenced by the Australian fires.

Long after the effects of the wildfire smoke dissipated in March of 2020, the ensemble average negative SST anomalies across the equatorial Pacific are sustained in lead year 3 with statistically significant anomalies approaching -0.8 °C in CESM2 (Fig. 1e, August 2021–July 2022) with a similar pattern in E3SMv2 but, again, about half the amplitude as in CESM2. Notably, areas of SST cooling are still present in the SPMM region in the southeast Pacific subtropics, most strongly in CESM2, with smaller negative anomalies in those regions in E3SMv2. As will be discussed later, these are the indications of a positive NPMM forming in lead year 3 in the CESM2 ensemble (Fig. 1e) but not in the E3SMv2 (Fig. 1f). Additionally, ensemble mean positive SST anomalies become established over the Maritime Continent, particularly in lead year 3 in both models (Fig. 1e, f) as seen in observations in typical La Niña events and during the triple-dip La Niña in the early 2020s[3].

As could be expected from these SST anomalies, there are corresponding negative precipitation anomalies extending across the equatorial Pacific, with statistically significant values in CESM2 of nearly -1.0 mm day^{-1} near and west of the Dateline in year 3 with positive precipitation anomalies over the Maritime Continent of about +0.6 mm day^{-1} (Fig. 2a) with similar-signed anomalies of smaller magnitude in E3SMv2 (Fig. 2b). Yellow and light blue circles in Figs. 2a and 3b highlight positive and negative precipitation anomalies, respectively, in comparable positions to those in observations[3]. As these SST and precipitation anomalies are sustained in lead year 3, sea level pressure (SLP) increases over the cooler water in the eastern tropical and subtropical Pacific with largest positive statistically significant values in lead year 3 up to about +0.7 hPa in CESM2 (Fig. 2c) with similar but lower amplitude anomalies in E3SMv2 (Fig. 2d). Meanwhile there are large statistically significant decreases of SLP over the warmer water near the Maritime Continent and southwestern tropical Pacific with values approaching -1 hPa in CESM2 (Fig. 2c) with, once again, similar sign but smaller amplitude anomalies in E3SMv2 (Fig. 2d).

The role of Bjerknes feedback

To turn to the question of why the initial La Niña conditions in the lead year 1 model sensitivity experiments were sustained out to lead year 3 in both models in the 30-year ensemble means, a major coupled feedback is the well-known Bjerknes feedback[26] which spreads and maintains the negative SST anomalies across the equatorial Pacific. For instance, stronger surface winds produce increased latent heat flux and increased upwelling of cooler water. Those negative SST anomalies are disproportionate in the central and eastern Pacific Ocean and result in an increased zonal SST gradient with positive SLP anomalies in the east that increase the meridional surface pressure gradient, which then strengthens the surface winds further, and so on. Observational evidence from the 2020–2023 La Niña showed that strong easterly surface wind anomalies associated with a strengthened zonal SST
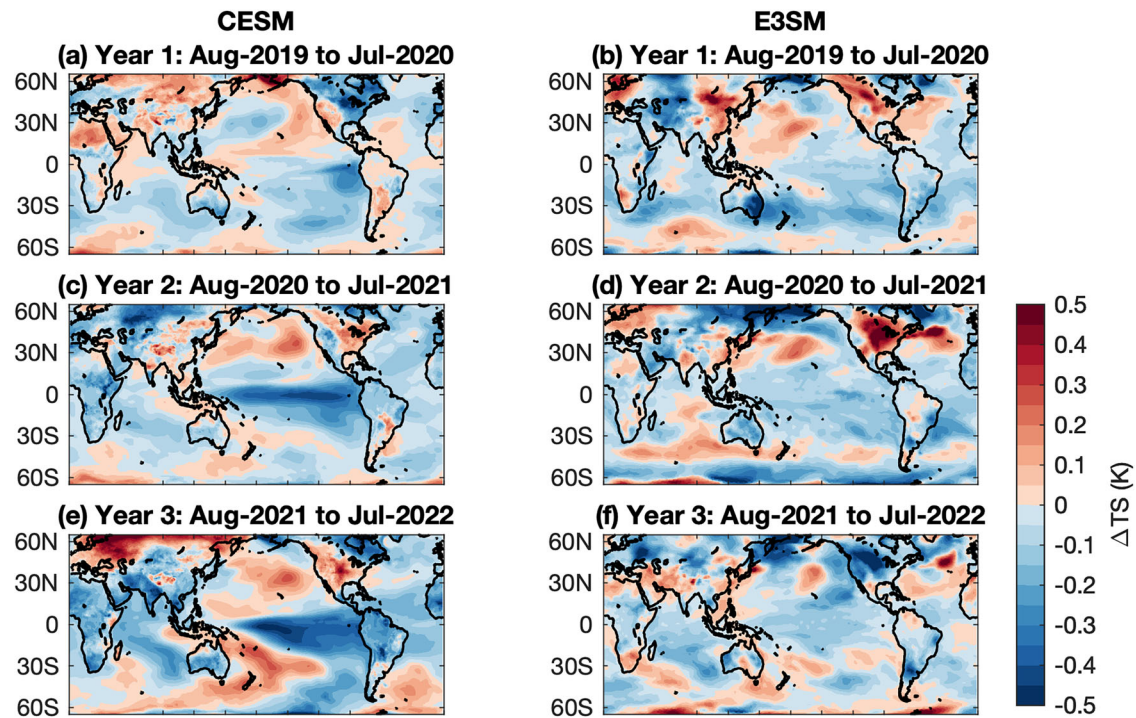
Fig. 1 | Surface temperature responses from the initialized hindcasts. 30-member ensemble means, smoke minus no-smoke, for CESM2 (left column) and E3SMv2 (right column), for August to July annual means for lead year 1 (**a, b**), lead year 2 (**c, d**), and lead year 3 (**e, f**) (°C). Lead year 1, 2, and 3 forecasts are initialized at the same time, August 2019, and here we look at the prediction after 1, 2, and 3 years (ensemble mean differences of smoke minus no-smoke runs). Anomalies greater in magnitude than about ±0.4 °C are significant at the 10% level from a two-sided *t*-test. Note that the magnitude of these anomalies is only qualitatively comparable to the anomalies from observations since the observations are anomalies from a climatology, while the model anomalies are differences between two initialized hindcasts for the same time period.


Fig. 2 | Lead year 3 responses. 30-member ensemble mean annual means from August 2021–July 2022, smoke minus no-smoke, for CESM2 (left column) and E3SMv2 (right column) for precipitation (**a, b**, anomalies greater in magnitude than about ±0.6 mm day^{-1} are significant at the 10% level from a two-sided *t*-test); sea level pressure (SLP, **c, d**, anomalies greater in magnitude than about ±0.2 hPa are significant at the 10% level) with surface wind arrows superimposed; and 200 hPa velocity potential (CHI, **e, f**, anomalies greater in magnitude than about ±0.3 × 10^6 m^2 s^{-1} are significant at the 10% level). Note that the magnitude of the anomalies in (**a, b**) is only qualitatively comparable to the anomalies from observations (e.g., McPhaden[3]) since the observations are anomalies from a climatology, while the model anomalies are differences between two initialized hindcasts for the same time period.
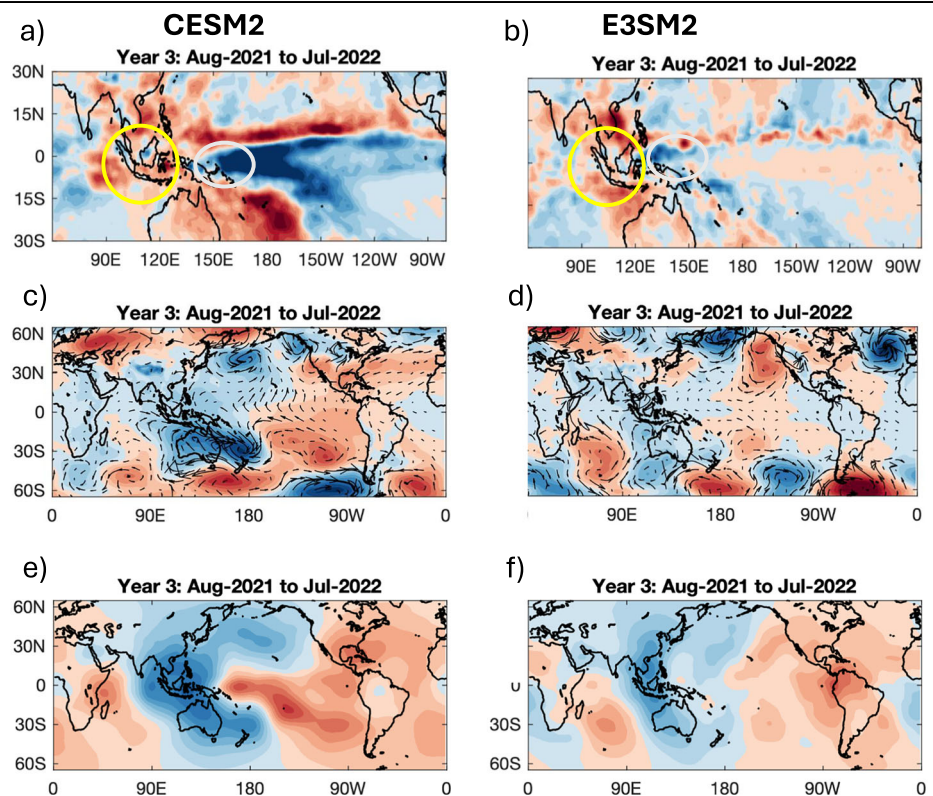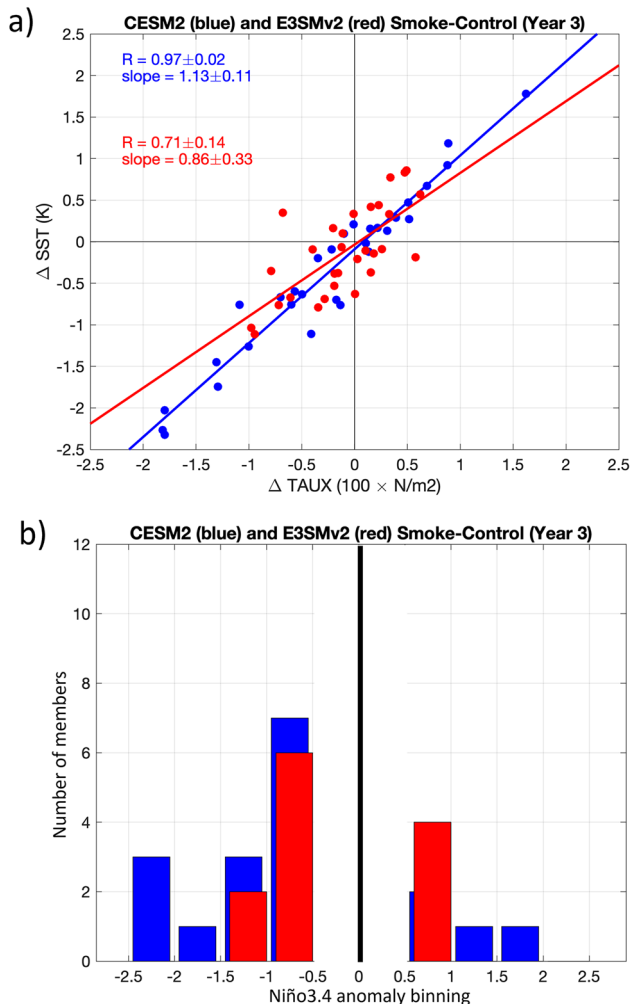
Fig. 3 | Bjerknes feedback and Niño3.4 SSTs. a Bjerknes feedback (*y*-axis) plotted as a function of surface wind stress gradient across the equatorial Pacific (*x*-axis) as defined in the text for each of the 30 ensemble members, smoke minus no-smoke; blue dots are CESM2, red dots E3SMv2; **b** half-degree bins of La Niña (negative values) and El Niño (positive values) ensemble members in (**a**) defined as Niño3.4 greater than ±0.5 °C for El Niño/La Niña, respectively, blue bars CESM2, red bars E3SMv2; The number of CESM2 members is greater than the number of E3SMv2 members because more of the latter distribution falls between −0.5 and 0.5.

gradient across the tropical Pacific helped maintain the event out to 3 years, though causality is difficult to establish from observations[3,5].

To quantify the intensity of this feedback[27] in the model hindcast experiments, the zonal SST gradient is defined as the difference of the SST anomaly for a western Pacific region (5°S–5°N and 110°E–150°E) that includes the Maritime Continent, minus an eastern Pacific region (5°N–5°S and 180°–110°W). The surface wind anomalies that power the Bjerknes feedback are quantified by a wind index consisting of the zonal (u component) surface wind stress anomalies averaged spatially across the equatorial Pacific basin (160°E–130°W; 5°S–5°N). A Bjerknes feedback that produces negative tropical Pacific SST anomalies has larger positive values for the west minus east SST difference (warm SSTs over the Maritime Continent, cooler SSTs over the Niño3.4 region), and larger negative values for the wind stress index, indicating anomalous easterlies.

As the La Niña continues in lead year 3 in the model simulations, there is an ensemble mean SST difference in CESM2 of +0.4 ± 0.2 °C (ranges are given as ± one standard deviation of the difference of sample means) and a same sign but lower value in E3SMv2 of +0.1 ± 0.1 °C (Fig. 1e, f). The ensemble mean wind stress index values for CESM2 and E3SMv2 are both

negative, −0.3 ± 0.2 Nm⁻² and −0.1 ± 0.1 Nm⁻², respectively. The SLP gradient across the Pacific that maintains the Bjerknes feedback is shown for year 3 in both models with statistically significant positive values greater than +0.2 hPa in the tropical eastern Pacific, and significant negative values less than −0.2 hPa over the Maritime Continent in the west (Fig. 2c, d). Thus, a strong Bjerknes feedback is still at work in the lead year 3 in both models in the response to the fires (i.e., their ensemble means). It feeds off the warmer SSTs in the west (Fig. 1e, f), consequent stronger precipitation over the Maritime Continent (yellow circles in Fig. 2a, b), and lower SLP (blue shading over the Maritime Continent in Fig. 2c, d) with higher SLP over the tropical Pacific (red shading in Fig. 2c, d).

The agent that connects the western Pacific/Maritime Continent region with the tropical eastern Pacific, thus driving the Bjerknes feedback in both models, which contributes to maintaining the cooler tropical Pacific SSTs into lead year 3, is the large-scale zonal atmospheric Walker Circulation[28]. The enhanced precipitation (yellow circles in Fig. 2a, b) over the warmer SSTs in the Maritime Continent region (Fig. 1e, f) produces greater vertical motion and upper-level outflow, shown by significant negative values of 200 hPa velocity potential there greater than −0.5 × 10⁶ m² s⁻¹ in both models (Fig. 2e, f). This connects to greater upper-level convergence over the tropical eastern Pacific (positive values of that magnitude in both models in Fig. 2e, f). The resulting anomalous descent then contributes to local positive SLP anomalies (Fig. 2c, d).

These changes of upper-level velocity potential, indicative of an intensification of the anomalous Walker Circulation between the western and eastern Pacific, contribute to the SLP anomalies (stronger ascent in the west associated with lower SLP, stronger descent in the east with higher SLP). Those SLP anomalies, in turn, drive the Bjerknes feedback with stronger surface easterlies that fuel stronger upwelling of cooler water, thus strengthening the negative SST anomalies over the equatorial Pacific[29], and so on. Therefore, the Bjerknes feedback involves a set of coupled processes that is able to maintain cooler SSTs across the tropical Pacific into lead year 3. This suggests that there could be a connection to longer-timescale decadal variability processes in the tropical Pacific.

Coupled processes linked to a multi-year negative IPO

There was an observed positive multi-year trend in off-equatorial ocean heat content in the western Pacific Ocean after the transition from positive to negative IPO around the year 2000 that indicated a buildup in ocean heat content that continued to about 2014 (Fig. S2). Previous evidence suggested that such a buildup of ocean heat content was necessary for a transition from negative to positive IPO triggered by an El Niño event to discharge that off-equatorial heat content[4]. In fact, evidence from observations indicated that such a transition had possibly occurred after the 2015–2016 El Niño event[30–33], and a model initialized in 2013 for predictions over the 2015-2019 period showed a transition to positive IPO in that time period[12,32]. Therefore, the drop in off-equatorial ocean heat content coincident with that El Niño event (Fig. S2) was consistent with the possible apparent start of an IPO transition from negative to positive with consequent predictability on the decadal timescale. But then there was an unexpected rise of off-equatorial ocean heat content that continued beyond 2020 (Fig. S2) and was coincident with the onset of a multi-year La Niña event in 2020[10,17]. However, the problem with attempting to assess decadal timescale transitions from interannual timescale data is that it is difficult to determine if a decadal transition has occurred until at least a few years after the fact. Therefore, Fig. S2 can only be interpreted as suggestive of decadal timescale conditions.

Given that caveat, there is a set of coupled feedbacks that could connect the multi-year La Niña to the IPO. These are a consequence of the La Niña-like conditions that survive into lead year 3 and involve processes in the western tropical Pacific that have been shown to be associated with the sustained negative phase of the IPO[12] and are typical of cold decadal epochs in the tropical Pacific[34]. Key elements of maintaining the multi-year time-scale of the IPO are coupled processes that contribute to the buildup of off-equatorial western Pacific Ocean heat content[4,12]. Negative SST anomalies and consequent negative precipitation anomalies in the western equatorial

Pacific produce negative convective heating anomalies that drive a Gill-type response in the atmosphere with anomalous surface highs to the north and south[4]. Consequently, there are positive wind stress anomalies near 25°N and 25°S in model composites from a long control run and in a specified convective heating anomaly experiment that produce Ekman pumping near 15°N–20°N and 15°S–20°S, and this produces increases in ocean heat content in those regions[4]. There is a similar response in lead year 3 in both CESM2 (Fig. S3a) and E3SMv2 (Fig. S3b) to the negative SST anomalies in the western equatorial Pacific (Fig. 1e, f) and consequent negative precipitation anomalies there (Fig. 2a, b, blue circles). These are also seen in the observed SST and precipitation anomalies (McPhaden[3]). There is a Gill-type response with anomalous surface highs to the north and south, and positive (westerly) surface wind stress anomalies near 15°–20°N and S (Fig. S3a, b). This wind stress forcing produces Ekman pumping near 15°N and 15°S[4] with a consequent significant increase in ocean heat content near 10°N and 10°S of more than $+0.2 \times 10^9$ Joules in those locations (Fig. S4a, b). These changes in off-equatorial ocean heat content amount to an increase of 173% and 325% from year 2 to year 3 in the north and south off-equatorial western Pacific areas, respectively, defined in Fig. S2 for CESM2, and increases of 60% and 123% in those areas in E3SMv2. Comparable increases are also seen in observations for this time period (Fig. S4c). The larger response south of the equator is related to a more coherent pattern of wind stress forcing as part of the anomalous high south of the equator compared to the north. Thus, as the La Niña event continues, these long-lived coupled feedbacks in the western Pacific begin to resemble the negative phase of the IPO, with those coupled feedbacks on the longer decadal timescale that could contribute to the long-lasting La Niña event[4].

Why does La Niña continue in lead year 3 in some ensemble members and not others?

If the Bjerknes feedback is the dominant mechanism for maintaining the multi-year La Niña in these two models with possible connections to the IPO, it would be useful to better quantify this feedback across the spread of 30 ensemble members for each model. Figure 3a is a scatter plot of Bjerknes feedback, defined earlier, as a function of Niño3.4 SSTs for DJF in year 3 for all 30 ensemble members for both models, shown as the difference between the smoke and no-smoke simulations. As expected, there is a strong positive correlation between Bjerknes feedback and Niño3.4 SSTs (correlation of 0.97 ± 0.02 for CESM2 and 0.71 ± 0.14 for E3SMv2, both at the 95% significance level). The stronger connection in CESM2 compared to E3SMv2 likely has contributions to the larger ENSO amplitude in CESM2, as noted earlier. Interestingly, in some ensemble members in both models, there is a shift toward El Niño in year 3 (as opposed to weaker La Niña) in Fig. 3a and illustrated in the histogram in Fig. 3b. Thus, the ensemble mean surface temperature responses in Fig. 1 reflect the shift toward 3-year La Niña in Fig. 3b among ensemble members with a large spread. For La Niña or El Niño, defined as Niño3.4 SSTs greater in magnitude than ±0.5°C, in CESM2 in year 3, there are 14 La Niña ensemble members vs 4 El Niño ensemble members, and for E3SMv2, there are 8 La Niña vs 4 El Niño ensemble members. This indicates that there are 2-year La Niña events that transition to El Niño in lead year 3, though there are many more ensemble members with 3-year events that stay as La Niña in lead year 3 with a strong positive Bjerknes feedback.

To examine these processes in more detail, we compile composites for the 5 strongest vs 5 weakest Niño3.4 anomalies (defined from Fig. 3a) for each model for a set of fields. The left column in Fig. 4 shows the "sustained"
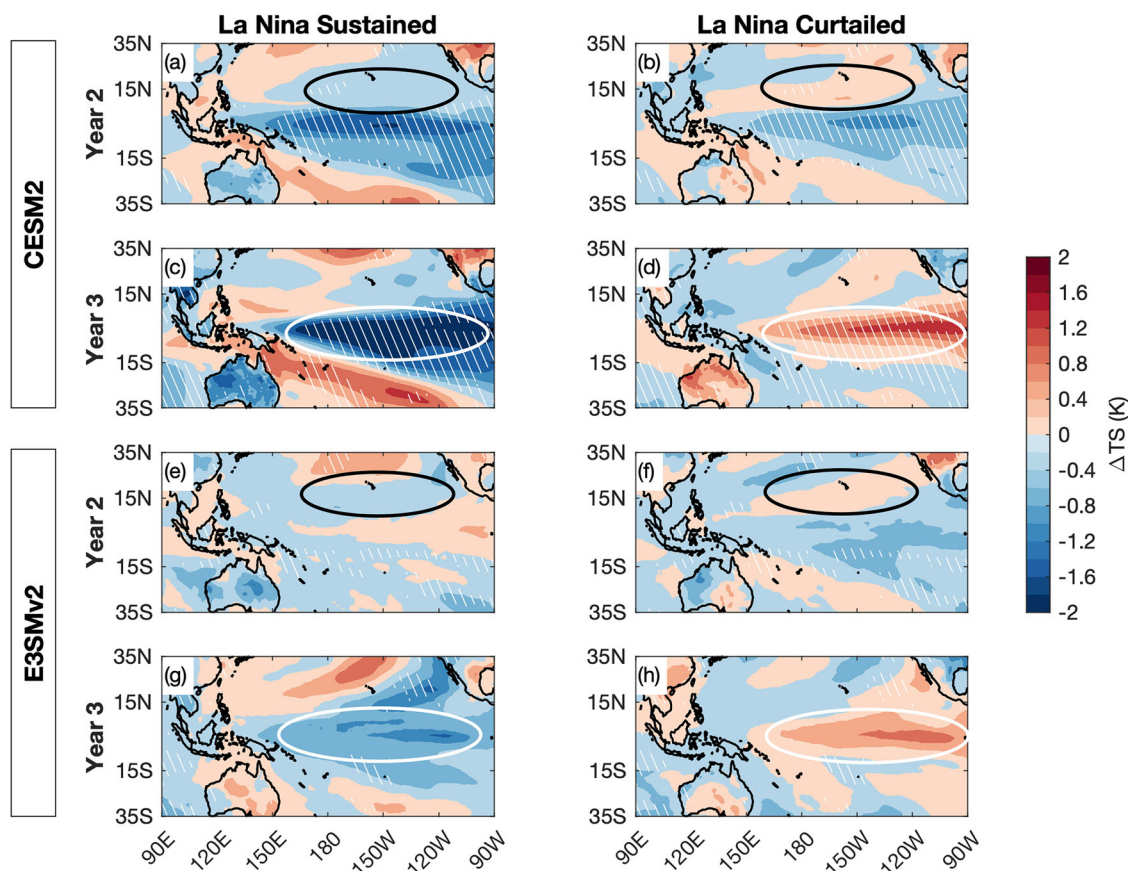

Fig. 4 | Surface temperature response for sustained versus curtailed multi-year La Niña. Five strongest 3-year sustained La Niña surface temperature anomalies (°C) from Fig. 3a (left column), and curtailed 2-year La Niña surface temperature anomalies from Fig. 3a (right column); **a, b**: lead year 2 CESM2; **c, d**: lead year 3 CESM2; **e, f**: lead year 2 E3SMv2; **g, h**: lead year 3 E3SMv2. Black ellipses in the first and third rows highlight anomalies associated with the NPMM in year 2, which affect the evolution of the equatorial Pacific anomalies during year 3 (white ellipses in rows 2 and 4). White hatching indicates significance at the 10% level from a two-sided t-test.
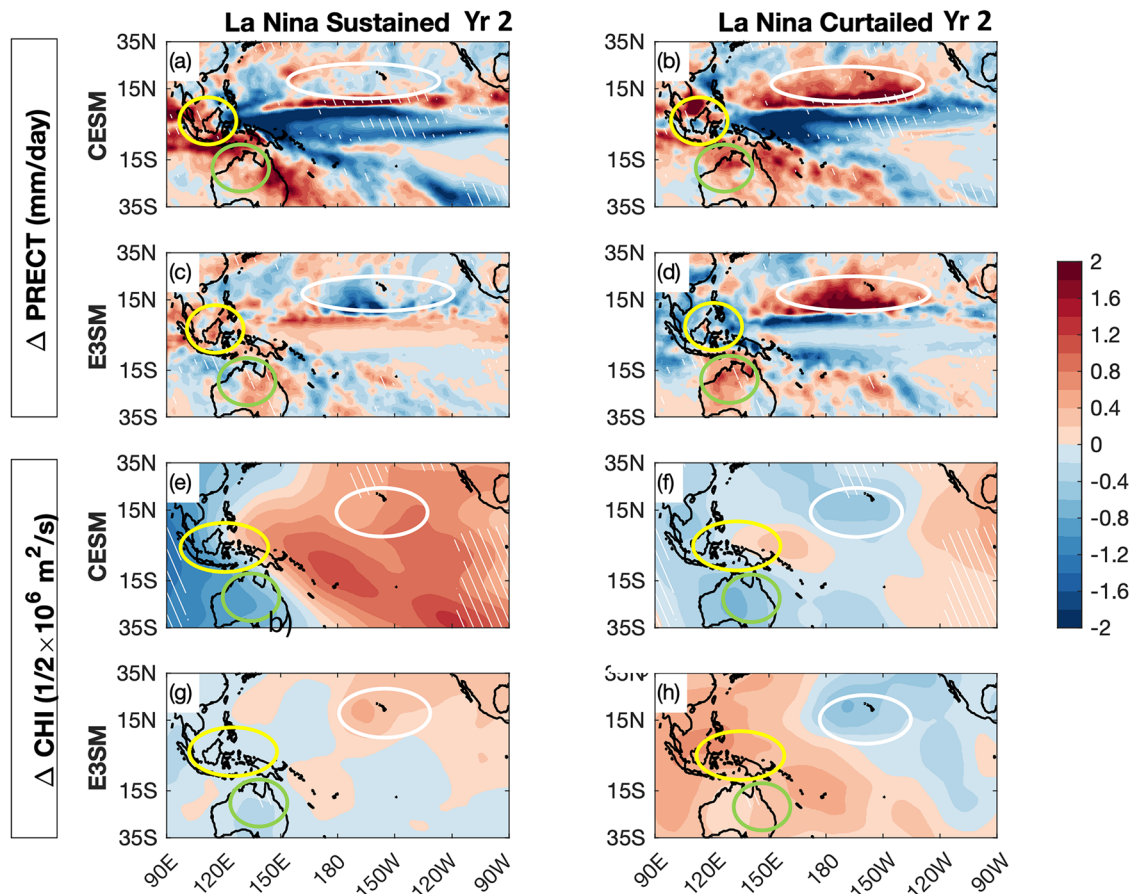
Fig. 5 | Conditions for sustained versus curtailed multi-year La Niña. Five strongest 3-year sustained La Niña conditions from Fig. 3a (left column), and curtailed 2-year La Niña conditions from Fig. 3a (right column); **a, b**: year 2 CESM2 precipitation (mm day^{-1}); **c, d**: year 2 E3SMv2 precipitation anomalies (mm day^{-1}); **e, f**: year 2 CESM2 200 hPa velocity potential (CHI, 10^6 m^2 s^{-1}); **g, h**: year 2 E3SMv2

200 hPa velocity potential (CHI, 10^6 m^2 s^{-1}). White hatching indicates significance at the 10% level from a two-tailed t-test. The 200 hPa velocity potential response in the sustained members of CESM2 is stronger than that in E3SMv2 due to the stronger changes in precipitation (**a**) in CESM2 compared to E3SM in (**c**).

3-year La Niña events, and the right column the "curtailed" La Niña 2-year events for each field.

Surface temperature anomalies for year 3 in the curtailed composite (i.e., in ensemble members that do not sustain a 3-year La Niña) show, consistent with Fig. 3, that these cases do not just correspond to a weaker La Niña in year 3, but a transition to El Niño that shuts off the La Niña event after lead year 2 (white ovals in Fig. 4d, h compared to Fig. 4c, g). To look for clues as to what sets the stage in year 2 for either a transition to El Niño or sustained La Niña, there is a band of positive SST anomalies near Hawaii and out past the Dateline from about 10°N to 20°N in yr 2 in the curtailed La Niña composite (Fig. 4b, f, black ovals) compared to negative SST anomalies in that region for sustained La Niña in both models (Fig. 4a, e, black ovals). This is manifested as a narrowing of the northern side of the negative SST anomaly pattern in the tropical eastern Pacific in lead year 2 (Fig. 4, black ovals). These positive SST anomalies in the curtailed composites arcing down from the northeast Pacific (Fig. 4b, f) resemble the positive pattern of the NPMM noted earlier, which is thought to be stochastically generated, though evidence presented here suggests in this instance it may be partially forced by the smoke. In any case, it has been shown to contribute to El Niño transitions as noted earlier[20–22]. Additionally, such a positive NPMM SST anomaly pattern has been shown to play a role in shutting off multi-year La Niña events in a hybrid coupled model[35].

Over those positive SST anomalies near Hawaii and the Dateline from about 10°N–20°N in lead year 2 (Fig. 4b, f), there are positive precipitation anomalies in the curtailed composite (Fig. 5b, d, white ovals) but not in the sustained composite (Fig. 5a, c, white ovals). Meanwhile, there is a relative

reduction of positive precipitation anomalies over the northern Maritime Continent in the lead year 2 curtailed composite (Fig. 5b, d, yellow circles) compared to the larger positive precipitation anomalies there in the lead year 2 sustained composite (Fig. 5a, c). Over the southern Maritime Continent and northern Australia, there are positive precipitation anomalies in lead year 2 in both the sustained composites (Fig. 5a, c, green circles) and the curtailed composites (Fig. 5b, d, green circles). Thus, in the sustained composites in both models, positive precipitation anomalies cover the entire Maritime Continent and northern Australia, while in the curtailed composites, only the southern part of the Maritime continent and northern Australia have large positive precipitation anomalies (Fig. 5).

Over the positive precipitation anomalies near Hawaii and the Dateline (15°N in lead year 2 for curtailed, Fig. 5b, d), there are negative 200 hPa velocity potential (CHI) anomalies (white ovals, Fig. 5f, h), indicating anomalous upper-level outflow above the stronger precipitation. This can be compared to positive CHI anomalies indicating relatively stronger upper-level convergence over that region in the sustained ensemble (Fig. 5e, g, white ovals) associated with neutral or slightly negative precipitation anomalies there (white ovals, Fig. 5a, c). There are weaker negative or positive CHI anomalies over the northern Maritime Continent for the curtailed ensembles (Fig. 5f, h, yellow ovals), indicating a relative increase in upper-level convergence compared to the sustained ensembles, and suppression of upward vertical motion associated with relative reductions of precipitation there (yellow ovals, Fig. 5b, d). Positive precipitation anomalies over the southern Maritime Continent and northern Australia are present in both models for the sustained and curtailed composites (Fig. 5a–d, green
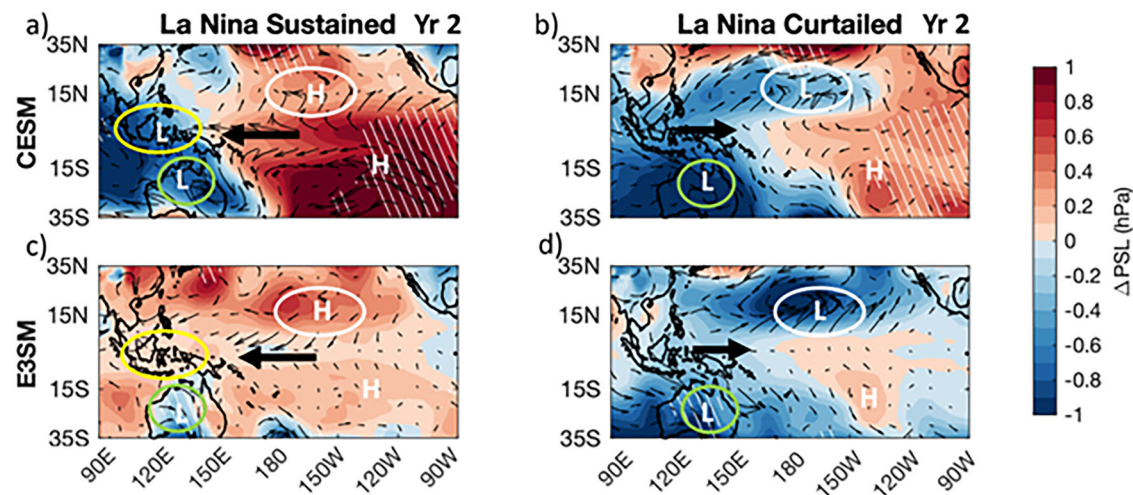
Fig. 6 | Atmospheric circulation response for sustained versus curtailed multi-year La Niña. Five strongest 3-year sustained La Niña conditions from Fig. 3a (left column), and curtailed 2-year La Niña conditions from Fig. 3a (right column); **a, b**: year 2 CESM2 sea level pressure anomalies (hPa), and 850 hPa wind anomaly vectors; **c, d**: year 2 E3SMv2 precipitation anomalies (mm day⁻¹) and 850 hPa wind anomaly vectors. White hatching indicates significance at the 10% level from a two-tailed *t*-test.

ovals). Those positive precipitation anomalies have corresponding negative or less positive CHI anomalies in the models in both the sustained and curtailed composites (Fig. 5e–h, green ovals), indicating enhanced vertical motion and upper-level outflow. This hemispheric asymmetry is an important aspect of why the curtailed composites transition to El Niño in lead year 3 and the sustained composites continue to a 3-year La Niña, as will be discussed below.

SLP anomalies for the curtailed ensembles for both models show negative anomalies in the areas near 15°N between the Dateline and Hawaii ("L" in white ovals, Fig. 6b, d) associated with the positive SST (Fig. 4b, f) and precipitation anomalies (Fig. 5b, d), and negative CHI anomalies there (Fig. 5f, h). Both the sustained and curtailed ensembles show ongoing negative SLP anomalies near northern Australia ("L" in green ovals, Fig. 6a–d) associated with positive SLP anomalies in the tropical southeast Pacific (denoted by white "H"). However, there are larger amplitude negative SLP anomalies in the curtailed ensembles over northern Australia ("L" in green ovals, Fig. 6b, d) as compared to the negative SLP anomalies to the north. This produces an anomalous meridional SLP gradient between the Maritime Continent and northern Australia with associated 850hPa westerly wind anomalies in the far western equatorial Pacific (Fig. 6b, d, highlighted by dark arrow). These westerly anomaly winds produce downwelling Kelvin waves that contribute to a previously well-documented[4] deepening of the thermocline in the eastern equatorial Pacific and a transition to positive SST anomalies in year 3 in the curtailed ensembles (Fig. 4d, h, white ovals). Meanwhile, in the sustained composites, there are positive SLP anomalies over the areas near 15°N between the Dateline and Hawaii in both models ("H" in white ovals, Fig. 6a, c) and an ongoing zonal SLP gradient between northern Australia and the central tropical Pacific south of the equator that combine to produce anomalous easterlies across the entire Pacific (dark arrows in Fig. 6a, c). These strong anomalous easterlies maintain a strong Bjerknes feedback (Fig. 3) and sustain the La Niña-like SST anomalies into the third year (Fig. 4c, g).

Therefore, the key difference between the curtailed and sustained composites, which starts a chain of coupled interactions that produces a transition to El Niño in lead year 3 in the curtailed composites and a continuing La Niña in lead year 3 in the sustained composites, is the positive NPMM SST anomaly pattern, that could be stochastically forced or have some contribution from the smoke forcing, which is established in the curtailed composites in lead year 2 near 15°N between the Dateline and Hawaii (Fig. 4b, f). These positive SST anomalies in the northern tropical Pacific then produce increased precipitation, lower SLP, and increased

upper-level outflow. The consequent anomalous Walker Circulation connects these anomalies with enhanced upper-level convergence over the northern Maritime Continent, a relative reduction of precipitation, and reduced magnitude negative SLP anomalies there. The anomalous negative SLP anomalies north of the equator in the central tropical Pacific combine with the ongoing anomalous Walker Circulation connecting the central tropical Pacific south of the equator to northern Australia, where there are stronger precipitation and negative SLP anomalies. The anomalous meridional SLP gradient in the far western equatorial Pacific then produces anomalous westerly component 850 hPa winds that contribute to downwelling Kelvin waves and the previously well-documented transition to El Niño conditions in lead year 3. Thus, the sign of the Bjerknes feedback reverses to positive in lead year 3 in the curtailed composites, while it remains negative in the sustained composites (Fig. 3; note that the ensemble members with the largest cooling (or warming) of Niño3.4 SSTs in Fig. 3a are represented in Fig. 3b).

The 30-member ensemble-mean off-equatorial western Pacific ocean heat content noted in Fig. S4 to characterize the negative phase of the IPO is reflected in changes for the sustained and curtailed ensemble means as well. As could be expected, the sustained ensemble mean, with an even greater negative IPO signature, shows an increase from lead year 2 to lead year 3 of 118% and 125% for the north and south areas, respectively, for CESM2, and increases of +433% and +184% for E3SMv2. Also, as could be expected, there are mostly reductions in lead year 3 in the curtailed 2-year La Niña events that transition to El Niño, with decreases of −546% and −85% in the north and south areas, respectively, in CESM2, and a decrease of −247% in the north area but an increase of +280% in the south area in E3SMv2, the latter mainly due to increases near 5°N associated with the El Niño onset.

Comparison to the observed early 2020s triple-dip La Niña

The observed early 2020s triple-dip La Niña lasted until roughly March 2023[7]. Since our lead year 3 hindcast covers the period August 2021 through July 2022, it misses the final 8 months of the observed event from August 2022 through March 2023. The question arises, what do the two models simulate for those months?

Time series of Niño3.4 SSTs for the observed SST anomalies are compared to smoke-minus-no smoke hindcast SST differences from the two models (Fig. 7). The timeline demarcations on the *x*-axis note the durations of our lead year designations from August to July, as well as the more canonical ENSO year designations from April to March[3]. To enable a direct comparison to the duration of the observed triple-dip La Niña, we
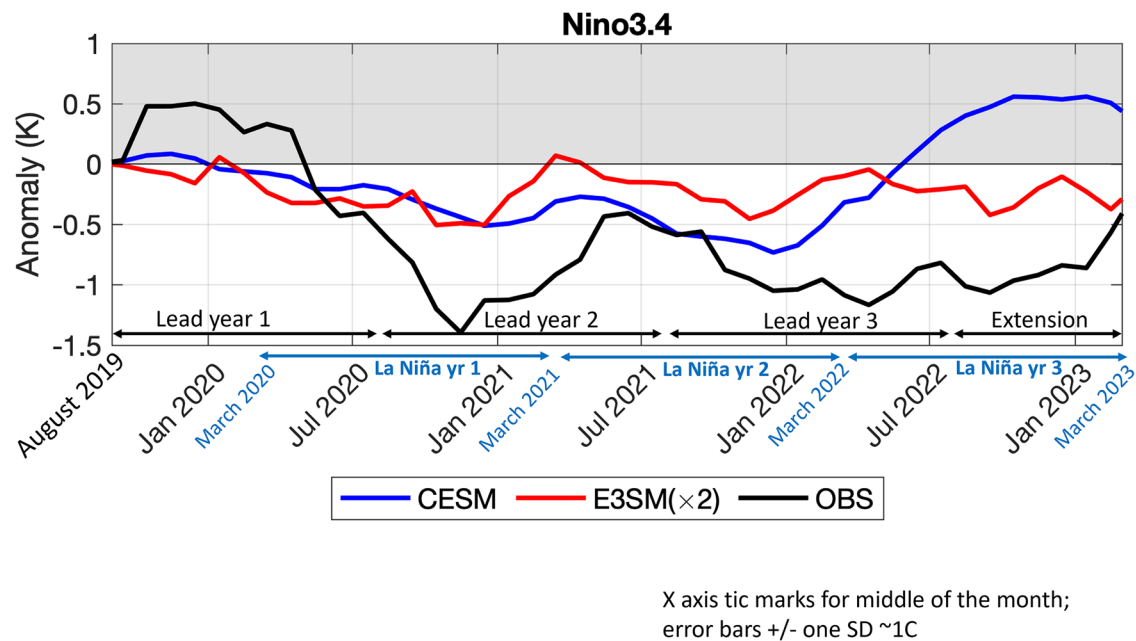
Fig. 7 | Niño3.4 time series. Monthly mean anomalies starting in August 2019 for observations (black line), CESM2 ensemble mean (blue line), and E3SMv2 ensemble mean (red line). Typical standard deviations for both models are roughly ±1 °C. Model hindcast years (e.g., lead year 1, etc.) are noted to start in August 2019 (black arrows) through lead year 3, and the extension from August 2022 through March 2023 is noted. For reference, canonical ENSO years (e.g., La Niña year 1) are noted to start in March 2020 (blue arrows) for the 3 years of the triple-dip La Niña.

extended the hindcasts to run from August 1, 2022 through March 2023. While E3SMv2 continues with negative values for the duration of the observed triple-dip event through March 2023, CESM2 transitions to El Niño in about April 2022 (Fig. 7), coinciding with the canonical timing of many observed La Niña events that transition to El Niño[7]. Figure S5 shows geographical plots of surface temperature differences from the two models for all lead years in the hindcasts with surface wind vector anomalies superimposed. These include the SST anomalies shown in Fig. 1, but add two additional panels for SST anomaly values averaged for the extension period from August 2022 through March 2023. As noted previously, the magnitude of the Niño3.4 SST difference values for E3SMv2 is about half that of the CESM2.

A contributing factor to the transition to El Niño that occurs in CESM2, which does not occur in E3SMv2, can be traced to lead year 3, where CESM2 shows the emergence of a positive NPMM pattern while E3SMv2 maintains the negative NPMM (noted in Fig. 1e, f, and also shown in Fig. S5e, f). As discussed above, transitions out of La Niña in the curtailed composites in both models (Fig. 4a–c, f) show the appearance of a positive NPMM in lead year 2, which then contributes to a transition to El Niño in lead year 3 in those composites with a positive NPMM. In the CESM2 extension beyond August 2022, the full ensemble shows positive NPMM in lead year 3 (Figs. 1e and S5e) that contributes to a transition to El Niño in the extension period (Fig. S5g). The ongoing negative NPMM in E3SMv2 (Figs. 1f and S5f) maintains the La Niña conditions through March 2023 (Fig. S5h) for comparable reasons to those documented in Figs. 5 and 6.

Discussion

The coupled feedbacks that maintain the La Niña conditions out to 3 years in the model ensemble mean simulations, which measure the climate system response to the Australian wildfire smoke, are summarized in Fig. 8. Recall that the only aspect of these initialized hindcasts that changes in the smoke simulations is the inclusion of observed Australian wildfire smoke emissions. These are compared to the standard no-smoke hindcasts that use a climatology of emissions. The processes associated with the initial response to the forcing from the Australian wildfire smoke that helped to initiate the La Niña event in 2020 are documented in detail[6,16] and reviewed here in Fig.

8, top. Australian wildfire smoke crosses the Pacific (labeled "1" in Fig. 8 top, and referred to here as [1]) and brightens the clouds off the coast of South America [2] by providing larger numbers of CCN that produce smaller cloud droplets and brighter, longer-lived clouds. These clouds reduce the incoming solar at the surface to cool the SSTs, driving cold anomalies that then propagate northward [3]. Those cooler SSTs in the eastern Pacific initiate coupled Bjerknes feedbacks that begin to spread the negative SST anomalies westward [4].

Then, a positive Bjerknes feedback maintains the La Niña conditions out to 3 years in the ensemble mean after the smoke anomalies have dissipated (Fig. 8, lower left). The strengthened Bjerknes feedback is characterized by stronger surface easterlies with stronger upwelling, which spreads the negative SST anomalies to the western equatorial Pacific. This is associated with a warming of SSTs and increased precipitation over the Maritime Continent [5] as seen in prior La Niña events. The upward vertical motion associated with stronger convection increases upper-level outflow, with a corresponding strengthening of upper-level convergence to the east and descent over the subtropical high region of the eastern Pacific, thus representing a stronger anomalous Walker Circulation [6]. The stronger descent from this intensified anomalous Walker Circulation contributes to a stronger South Pacific high and increased southeast trade winds [7]. Once begun, these coupled feedbacks can maintain the La Niña/negative IPO state until something happens to cause a transition. In the observations and previously analyzed model simulations, that is often an El Niño event[4], and this is the case here for the 2-year events.

Analysis of the strongest sustained La Niña ensemble members, compared to the strongest ensemble members that do not sustain a 3-year La Niña, shows the latter transitions to El Niño after lead year 2 in both models (Fig. 8, lower right). This is a result of positive NPMM SST anomalies in the northern tropical Pacific in those ensemble members that could be stochastically generated or partially forced by the smoke, which weakens the anomalous Walker Circulation north of the equator, while the Walker circulation remains strong south of the equator. This hemispheric asymmetry in the far western Pacific contributes to westerly surface wind anomalies in the equatorial western Pacific, and a transition to El Niño in those ensemble members in lead year 3. However, there is a preponderance
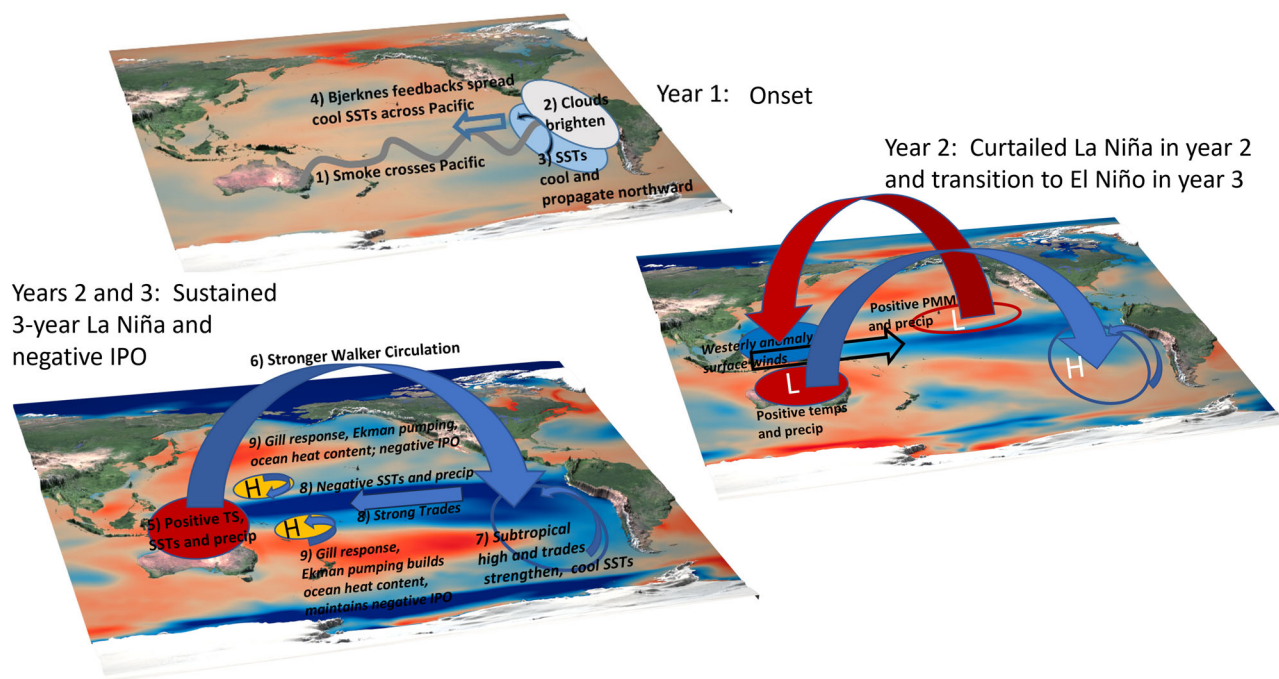
Fig. 8 | Coupled interactions for multi-year La Niña triggered by Australian wildfire smoke in 2019–2020. Top: year 1 onset; (1) wildfire smoke crosses the Pacific where it reaches the eastern Pacific, (2) brightens clouds there that (3) reflect more solar radiation to cool SSTs that propagate into the equatorial eastern Pacific where (4) Bjerknes feedbacks spread the negative SST anomalies westward (background SST anomalies from Fig. 1); Bottom left: in years 2 and 3, Bjerknes feedbacks spread negative SST anomalies across the Pacific and contribute to (5) increasing SSTs and precipitation over the Maritime Continent and northern Australia. The consequent enhanced vertical motion there then produces stronger upper-level outflow, (6) a stronger anomalous Walker Circulation with enhanced upper-level convergence over the eastern subtropical Pacific, and (7) a stronger subtropical high and stronger trade winds to maintain cool SSTs. Coupled feedbacks associated with the negative phase of the IPO in the western tropical Pacific result from (8) negative precipitation and convective heating anomalies over the anomalously cool water, (9) a Gill-type response with anomalous highs (yellow ovals) to the north and south, easterly wind stress anomalies in the near equatorial western Pacific, and westerly wind stress anomalies near 25°N and 25°S (blue arrows); these wind stress anomalies result in anomalous Ekman pumping near 15°–20°N and 15°–20°S which increases off-equatorial western Pacific ocean heat content characteristic of extended negative IPO-type conditions (background SST anomalies from Fig. 4a); Bottom right: For 2-year La Niña events that transition to El Niño in year 3, a positive NPMM north of the equator in the tropical Pacific produces positive precipitation and negative SLP anomalies (red oval), anomalous upper-level outflow with upper-level convergence over the Maritime Continent to the west (red ribbon arrow) with relatively higher surface pressure there (solid blue oval). Meanwhile, positive anomalies of surface temperature and precipitation and negative surface pressure anomalies over Australia (solid red oval) sustain the anomalous Walker Circulation to the east (blue ribbon arrow) with stronger descent and an anomalously strong South Pacific High (blue oval) with stronger trades in the equatorial eastern Pacific. The larger negative SLP anomalies over Australia set up an anomalous meridional SLP gradient that contributes to anomalous westerly surface winds in the far western equatorial Pacific (black arrow) that leads to a transition to El Niño in the third year (background SST anomalies from Fig. 4b).

of ensemble members in both models that show ongoing La Niña conditions in lead year 3 with a strong anomalous Bjerknes feedback that sustains the pattern.

A second set of coupled feedbacks in the western tropical Pacific (Fig. 8, lower left), with implications for the IPO, results from *[8]* negative precipitation anomalies over the anomalously cool water, and negative convective heating anomalies there. This produces *[9]* a Gill-type response with anomalous highs (yellow ovals) to the north and south, with easterly wind stress anomalies in the near equatorial western Pacific, and westerly wind stress anomalies near 25°N and 25°S (blue arrows). These wind stress anomalies result in Ekman pumping near 15°N–20°N and 15°S–20°S that increases off-equatorial western Pacific Ocean heat content. These anomalies are associated with extended negative IPO-type conditions and set the stage for a subsequent IPO transition[4].

To better compare with the duration of the observed triple-dip La Niña, extensions are run with both models from August 2022 through March 2023. The appearance of a positive NPMM in lead year 3 in CESM2 leads to a transition to El Niño in the extension period (as in Fig. 8, right), while an ongoing negative NPMM in lead year 3 in E3SMv2 maintains the La Niña-like conditions through March 2023 (as in Fig. 8, lower left).

An interesting feature of this two-model analysis is that while both models portray the same set of coupled feedbacks and processes with similar-signed anomalies and comparable patterns, the magnitudes of the signals in E3SMv2 are about half those in CESM2. The exact reason for this aspect of the results is beyond the scope of the present paper. But it could be related to coupled responses that are stronger in CESM2, whereby, for example, ENSO amplitude in CESM2 is about twice as large as observed[36] and twice as large as in E3SMv2[37]. Additionally, the relevant cloud-aerosol processes related to the smoke forcing in CESM2 are about twice the magnitude as in E3SMv2 (Fig. S1). In any case, we have presented evidence that the coupled processes triggered by the Australian wildfire smoke produce a prolonged multi-year La Niña-like set of anomalies in both E3SMv2 and CESM2.

Methods
CESM2 and E3SMv2
We focus on two models, E3SMv2 and CESM2, to illustrate in more detail how differences in the model responses to Australian wildfire smoke can affect coupled processes involved with a multi-year La Niña in those two models. Such "two model analyses" present advantages to understanding processes and thus have a rich history in the literature[38]. A single model analysis has no larger interpretability context because the results are from only one model's representation of the system. A multi-model ensemble analysis like CMIP can describe phenomena from a larger number of models, but a lack of knowledge of the details of all the models can only provide information on the "what" and little on the "why." A two-model analysis takes advantage of familiarity with the processes in the two models to provide more well-informed insights into the relative magnitudes of the

responses and the relevant physical mechanisms[37,39]. The atmospheric models in CESM2 and E3SMv2 have a nominal 1° latitude-longitude resolution[40,41]. CESM2 has a version of the Morrison Gettelman (MG1) microphysics scheme updated to MG2 in CESM2 that predicts precipitating hydrometeors. The model aerosol scheme includes an aging process for black carbon and has 4 modes (MAM4). The atmospheric model in E3SMv2 has a dynamical core that includes semi-Lagrangian tracer transport. Clouds Unified By Binormals, a high-order turbulence closure scheme, is used for subgrid turbulent mixing and cloud macrophysics in E3SMv2 and CESM2. Smoke and its interactions with clouds and radiation are represented in both CESM2 and E3SMv2. Smoke particles include both the scattering effects of organic matter and the absorbing effects of black carbon[16].

The case study sensitivity experiment hindcasts
The reference hindcasts for our experiments, termed "no smoke" here, are from the SMYLE experiments[18] with CESM2 and E3SMv2 with prescribed SSP3-7.0 climatological fire emissions. For both models, the full suite of SMYLE experiments consists of 2-year-long hindcast simulations that span the period from 1970 to 2019, with seasonal initializations within each year. However, for the Australian wildfire case study, we use the initial time of August 2019 for both sets of hindcasts (around the time when the wildfires started), and then the hindcasts are run for 3 years with a 30-member ensemble for each, with 30 ensemble member extensions from August 2022 through March 2023. The SMYLE experiments with both models are initialized with data from the Japanese 55-year reanalysis interpolated onto the CESM2 and E3SMv2 atmospheric grids. The land initial conditions come from a TRENDY-forced land simulation. The ocean and sea ice initial conditions are based on the forced ocean–sea ice simulations, constructed in line with the protocol for version 2 of the Ocean Model Intercomparison Project. SMYLE simulations are forced by smoothed biomass burning emissions, characterized by a mean climatological cycle of the satellite era, which are substituted for the default biomass burning emissions.

For the sensitivity experiment that includes the Australian smoke aerosols, the observed bushfire smoke emissions from GFED are included and termed the "smoke" hindcasts. Results here are shown for annual averages, August to July, computed as differences "smoke minus no-smoke" to see what effect the smoke had on the predictions. CESM2 and E3SMv2 both include aerosol schemes whereby CCN and cloud albedo can be affected by smoke aerosols such that the presence of smoke aerosols generally makes clouds brighter[6,16].

Drift of initialized hindcasts is a feature of such experiments and is typically removed using some drift correction method[32]. Drift is also present in the "no-smoke" and "smoke" hindcasts. However, ensemble differencing of the "smoke" and "no-smoke" experiments run in parallel over the same time period implicitly removes the drift.

Statistical significance is calculated from a two-sided t-test.

Data availability
E3SMv2 model code and tools may be accessed on the GitHub repository at https://github.com/E3SM-Project/E3SM. A maintenance branch (maint-2.0; https://github.com/E3SM-Project/E3SM/tree/maint-2.0) has been specifically created to reproduce E3SMv2 simulations. Complete native model output is accessible directly on NERSC at https://portal.nersc.gov/archive/home/projects/e3sm/www/WaterCycle/E3SMv2/LR. A subset of the data reformatted following CMIP conventions is available through the DOE Earth System Grid Federation (ESGF) at https://esgf-node.llnl.gov/projects/e3sm. The CESM2 datasets used in this study are available from the Earth System Grid Federation (ESGF) at esgf-node.llnl.gov/search/cmip6, or from the NCAR Digital Asset Services Hub (DASH) at data.ucar.edu, or from the links provided from the CESM website at www.cesm.ucar.edu. The Global Fire Emissions Database (GFED) smoke aerosol data are available from: https://www.globalfiredata.org/data.html. The ERA-5 data[42] are available from: https://www.ecmwf.int/en/forecasts/dataset/ecmwf-reanalysis-v5. ERSSTv5 data are available from: https://SLP.noaa.gov/data/gridded/data.noaa.ersst.v5.html. HADiSST data are available from: https://www.metoffice.gov.uk/hadobs/hadisst/. MERRA2 data from 1980-2015 (Doi:10.5065/D62R3QFS). GPCP rainfall data[43] are from https://www.esrl.noaa.gov/psd/data/gridded/data.gpcp.html.

References

1. Huang, A. T., Gillett, Z. E. & Taschetto, A. S. Australian rainfall increases during multi-year La Niña. *Geophys. Res. Lett.* **51**, e2023GL106939 (2024).
2. NOAA. Recent "Triple-Dip" La Niña upends current understanding of ENSO. https://research.noaa.gov/recent-triple-dip-la-nina-upends-current-understanding-of-enso/ (2023).
3. McPhaden, M. J. The 2020–22 triple-dip La Niña [in "State of the Climate in 2022"]. *Bull. Am. Meteor. Soc.* **104**, S157–S158 (2023).
4. Meehl, G. A., Teng, H., Capotondi, A. & Hu, A. The role of interannual ENSO events in decadal timescale transitions of the Interdecadal Pacific Oscillation. *Clim. Dyn.* https://doi.org/10.1007/s00382-021-05784-y (2021).
5. Li, X., Hu, Z.-Z., McPhaden, M. J., Zhu, C. & Liu, Y. Triple-dip La Niñas in 1998–2001 and 2020–2023: impact of mean state changes. *J. Geophys. Res. Atmos.* **128**, e2023JD038843 (2023).
6. Fasullo, J. T., Rosenbloom, N. & Buchholz, R. A multiyear tropical Pacific cooling response to recent Australian wildfires in CESM2. *Sci. Adv.* **9**, eadg1213 (2023).
7. Chen, H. C. et al. Understanding the driving mechanisms behind triple-dip La Niñas: insights from the prediction perspective. *npj Clim. Atmos. Sci.* **8**, 143 (2025).
8. DiNezio, P. N., Deser, C., Okumura, Y. & Karspeck, A. Predictability of 2-year La Niña events in a coupled general circulation model. *Clim. Dyn.* **49**, 4237–4261 (2017).
9. Kim, J. W., Yu, J. Y. & Tian, B. Overemphasized role of preceding strong El Niño in generating multi-year La Niña events. *Nat. Commun.* **14**, 6790 (2023).
10. Hasan, N. A., Chikamoto, Y. & McPhaden, M. J. The influence of tropical basin interactions on the 2020–2022 double-dip La Niña. *Front. Clim.* **4**, 1–13 (2022).
11. Wills, R. C. J., Dong, Y., Proistosecu, C., Armour, K. C. & Battisti, D. S. Systematic climate model biases in the large-scale patterns of recent sea-surface temperature and sea-level pressure change. *Geophys. Res. Lett.* **49**, e2022GL100011 (2022).
12. Meehl, G. A., Hu, A. & Teng, H. Initialized decadal prediction for transition to positive phase of the Interdecadal Pacific Oscillation. *Nat. Commun.* **7**, https://doi.org/10.1038/NCOMMS11718 (2016).
13. Wang, B. et al. Understanding the recent increase in multiyear La Niñas. *Nat. Clim. Change* **13**, 1075–1081 (2023).
14. Izumo, T. et al. Influence of the state of the Indian Ocean Dipole on the following year's El Niño. *Nat. Geosci.* **3**, 168–172 (2010).
15. Rodriguez-Fonseca, B. et al. Are Atlantic Niños enhancing Pacific ENSO events in recent decades? *Geophys. Res. Lett.* https://doi.org/10.1029/2009GL040048 (2009).
16. Fasullo, J. T. et al. Coupled climate responses to recent Australian wildfire and COVID-19 emissions anomalies estimated in CESM2. *Geophys. Res. Lett.* **48**, e2021GL093841 (2021).
17. Jiang, S., Zhu, C., Hu, Z.-Z., Jiang, N. & Zheng, F. Triple-dip La Niña in 2020-2023: Understanding the role of the annual cycle in tropical Pacific SST. *Environ. Res. Lett.* **18**, 084002 (2023).
18. Yeager et al. The Seasonal-to-Multiyear Large Ensemble (SMYLE) prediction system using the Community Earth System Model version 2. *Geosci. Model Dev.* **15**, 6451–6493 (2022).
19. Espinosa, Z. I. & Zelinka, M. D. The shortwave cloud-SST feedback amplifies multi-decadal Pacific sea surface temperature trends: implications for observed cooling. *Geophys. Res. Lett.* **51**, e2024GL111039 (2024.

Article

20. Di Lorenzo, E. et al. ENSO and meridional modes: a null hypothesis for Pacific climate variability. *Geophys. Res. Lett.* **42**, 9440–9448 (2015).
21. You, Y. & Furtado, J. C. The South Pacific Meridional Mode and its role in tropical Pacific climate variability. *J. Clim.* https://doi.org/10.1175/JCLI-D-17-0860.1 (2018).
22. Liguori, G. & Di Lorenzo, E. Separating the North and South Pacific Meridional Modes contributions to ENSO and tropical decadal variability. *Geophys. Res. Lett.* **46**, 906–915 (2019).
23. Shi, L., Ding, R., Hu, S., Li, X. & Li, J. Extratropical impacts on the 2020–2023 Triple-Dip La Niña event. *Atmos. Res.* **294**, 106937 (2023).
24. Iwakiri, T. et al. Triple-dip La Niña in 2020–23: North Pacific atmosphere drives 2nd year La Niña. *Geophys. Res. Lett.* **50**, e2023GL105763 (2023).
25. Zhang, S., Fan, H., Hu, X. & Lin, S. Unprecedented cross-equatorial southerly wind anomalies during the 2020–2023 triple-dip La Niña: impacts and mechanisms. *Atmos. Res.* **304**, 107–412 (2024).
26. Bjerknes, J. Atmospheric teleconnections from the equatorial Pacific. *Mon. Weather Rev.* **97**, 163–172 (1969).
27. Zheng, F., Fang, X.-H., Zhu, J., Yu, J.-Y. & Li, X.-C. Modulation of Bjerknes feedback on the decadal variations in ENSO predictability. *Geophys. Res. Lett.* **43**, 12,560–12,568 (2016).
28. Meehl, G. A. The annual cycle and interannual variability in the tropical Pacific and Indian Ocean regions. *Mon. Weather Rev.* **115**, 27–50 (1987).
29. England, M. H. et al. Slowdown of surface greenhouse warming due to recent Pacific trade wind acceleration. *Nat. Clim. Change* **4**, 222–227 (2014).
30. Hu, S. & Fedorov, A. V. The extreme El Niño of 2015–2016 and the end of global warming hiatus. *Geophys. Res. Lett.* **44**, 3816–3824 (2017).
31. Su, J., Zhang, R. & Wang, H. Consecutive record-breaking high temperatures marked the handover from hiatus to accelerated warming. *Sci. Rep.* **7**, 43735 (2017).
32. Meehl, G. A. et al. The effects of bias, drift, and trends in calculating anomalies for evaluating skill of seasonal-to-decadal initialized climate predictions. *Clim. Dyn.* https://doi.org/10.1007/s00382-022-06272-7 (2022).
33. Capotondi, A. & Qiu, B. Decadal variability of the Pacific shallow overturning circulation and the role of local wind forcing. *J. Clim.* **36**, 1001–1015 (2023).
34. Capotondi, A. et al. Mechanisms of tropical Pacific decadal variability. *Nat. Rev. Earth Environ.* **11**, 754–769 (2023).
35. Dong, X. et al. Thermodynamic processes prolong triple La Niña events in a hybrid coupled ocean-atmosphere model. *Clim. Dyn.* https://doi.org/10.1007/s00382-024-07564-w (2025).
36. Capotondi, A. et al. ENSO and Pacific decadal variability in CESM2. *J. Adv. Model. Earth Syst.* https://doi.org/10.1029/2019MS002022 (2020).
37. Meehl, G. A. et al. Climate base state influences on South Asian monsoon processes derived from analyses of E3SMv2 and CESM2. *Geophys. Res. Lett.* **50**, e2023GL104313 (2023).
38. Baumhefner, D. A single forecast comparison between the NCAR and GFDL general circulation models. *Mon. Weather Rev.* **104**, 1175–1177 (1976).
39. Meehl, G. A. et al. Processes that contribute to future South Asian monsoon differences in E3SMv2 and CESM2. *Geophys. Res. Lett.* **51**, e2024GL109056 (2024).
40. Danabasoglu, G. et al. The Community Earth System Model version 2 (CESM2). *J. Adv. Model. Earth Syst.* **12**, e2019MS001916 (2020).
41. Golaz, J.-C. et al. The DOE E3SM Model Version 2: overview of the physical model. *J. Adv. Model. Earth Syst.* **14**, e2022MS003156 (2022).
42. Hersbach, H. et al. The ERA5 global reanalysis. *Q. J. R. Meteorol. Soc.* **146**, 1999–2049 (2020).
43. Adler, R. F. et al. The Version 2 Global Precipitation Climatology Project (GPCP) Monthly Precipitation Analysis (1979-Present). *J. Hydrometeorol.* **4**, 1147–1167 (2003).

Author contributions
G.M. formulated the research and wrote the main manuscript text. A.G. prepared the figures. All authors contributed to the research tasks and helped to write and edit the manuscript.

Competing interests
The authors declare no competing interests.

Additional information
Supplementary information The online version contains supplementary material available at https://doi.org/10.1038/s41612-025-01204-8.

Correspondence and requests for materials should be addressed to Gerald A. Meehl.

Reprints and permissions information is available at http://www.nature.com/reprints

Publisher's note Springer Nature remains neutral with regard to jurisdictional claims in published maps and institutional affiliations.